Estimating microplastic concentrations in surface water using satellite-based turbidity measurements: a case study on the New River, VA

Luisana Rodriguez Sequeira

Thesis submitted to the faculty of the Virginia Polytechnic Institute and State University in partial fulfillment of the requirements for the degree of

Master of Science
In
Geoscience

George H. Allen, chair
Austin D. Gray, co-chair
Madeline E. Schreiber

April 29, 2025
Blacksburg, VA

Keywords: Microplastic pollution, remote sensing, water quality, proxy modeling

Estimating microplastic concentrations in surface water using satellite-based turbidity measurements: a case study on the New River, VA

Luisana Rodriguez Sequeira

ABSTRACT

Microplastic (<5 mm) pollution in rivers poses a threat to ecosystems and human livelihood around the world, yet the methods used to quantify and monitor their occurrence, distribution, and transport are highly limited. A substantial portion of plastics make their way into rivers through a variety of pathways such as direct dumping and environmental transport processes (wind, surface runoff, etc.). To detect and quantify microplastic abundance in rivers, traditional detection methods rely on visual observation and enumeration techniques, resulting in error due to bias in counting. These methods are time-consuming and require laborious field collection and laboratory work, inhibiting high-frequency observations over large spatial extents, which is needed to better understand the sources, sinks, and dynamics of microplastic pollution in waterways. Satellite remote sensing can provide regular water quality estimates in rivers with large spatial and temporal coverage, and we could use these estimates as a proxy for surface river microplastic concentrations. In this study, we relate the satellite-derived normalized difference turbidity index (NDTI) to co-temporal *in situ* turbidity and surface water microplastic concentrations. We focused our study on the New River, in Southwest Virginia, USA. Over the course of a year (September 2023 - September 2024), we collected and analyzed over 100 co-temporal water quality measurements, surface water microplastic concentration samples, and corresponding observations from satellite imagery. Using linear regression, we derived a relationship between NDTI and *in situ* turbidity that explains 71% of the variance ($R^2 = 0.71$). Seasonal relationships varied between *in situ* turbidity and microplastic concentrations which varied between R^2 0.19 and 0.56. We combined the equations relating NDTI, *in situ* turbidity, and co-temporal microplastic concentrations to directly relate satellite-derived NDTI to microplastic concentrations. With this equation, we can estimate microplastic concentrations along the New River on clear-sky days using Sentinel-2 at 10-m resolution, allowing us to delineate microplastic concentrations along the river. The method developed here can be used to advance our ability to track the dynamics of microplastic for improved assessments of sources and sinks of mismanaged plastic waste in Earth's waterways.

Estimating microplastic concentrations in surface water using satellite-based turbidity measurements: a case study on the New River, VA

Luisana Rodriguez Sequeira

GENERAL AUDIENCE ABSTRACT

Microplastics (<5mm), are pervasive in Earth's environments, and rivers are a major transport pathway. Microplastic detection methods that rely on counting individual particles are time-consuming and require laborious field collection, inhibiting real-time insights over large spatial extents, which are needed in order to better understand where microplastics go within inland rivers. Satellite remote sensing has been used to estimate inland water quality at relatively high spatial and temporal coverage. Thus, finding a correlation between water quality and microplastic concentration could allow us to estimate microplastic concentrations in rivers via satellite imagery using water quality as a proxy. We focused our study on the New River near Blacksburg, VA, and collected over 100 co-temporal water quality measurements and surface-water microplastic samples between September 2023 through September 2024. We combined these in situ measurements with co-temporal remotely sensed water quality index observations from Sentinel-2 to develop a model estimating microplastic concentration from satellite imagery. By providing more observations than what can be done with in situ sampling alone, we can improve large-scale microplastic analyses and modeling leading to better assessments of mismanaged plastic waste in Earth's rivers.

DEDICATION

to my family and my wonderful friends

who offer unwavering support and love

ACKNOWLEDGEMENTS

I would like to thank my co-advisor, Dr. George H. Allen, for giving me the opportunity to research a deep interest of mine—plastic pollution—and offering me guidance while I learned the wonders of satellite imagery analysis. I would also like to deeply thank my co-advisor, Dr. Austin D. Gray, for guiding me through the new world of toxicology research and always offering honest and experienced advice.

I am tremendously grateful for my many wonderful lab mates from both the Global Rivers Group and the Gray Lab at Virginia tech – Dr. Katie McQuillan, Molly Stroud, Emily Ellis, Yohtaro Kobayashi, Carter Boyd, David Go, Hana Thurman, Christine Cornish, Kathleen Mayer, Megan Gaesser, and Beija Gore. While accompanying me in the field and pushing me to participate in extracurricular activities, my lab mates showed me what it means to be supported within a community. I am especially thankful for having the honor of getting Dr. Katie McQuillan as my lab's post doc, desk mate, and neighbor. Life in Blacksburg would not have come close to being as enjoyable and comforting if she was not around.

I would also like to deeply thank the undergraduates that helped me in the field and lab – Jason Gross, Shaurya Prakash, and Julia Shelton. I am indebted to the work you all put into this research project and would not be where I am without your long hours of work.

I am deeply grateful for the VT Latinx communities I have found (LAIGSA and SACNAS) and been able to grow (La Plaga) with friends such as Gala Lucia Gonzalez Barrios. I would not have been able to call this place my home if it weren't for these groups.

Finally, I would like to thank the Virgina Tech graduate school for funding my last year of research and partially supporting me through the summer, and Dr. George H. Allen who supported the rest of my research through his startup fund.

Table of Contents

1. Introduction

Microplastics (<5 mm; MPs) have been found in nearly all ecosystems on earth, though there is still a dearth of knowledge regarding their transport through environments over time (Hale et al., 2020). There is more than 400 Mt of plastic produced each year, and about 20% is mismanaged, meaning it is discarded in a non-ecofriendly way (Geyer et al., 2017; OECD, 2024). MPs can either be intentionally manufactured, as primary MPs, or be created, as secondary MPs, by breaking off other plastic items (Lindeque et al., 2020). Plastic material creates secondary MPs through processes such as physical abrasion, microbial biodegradation, and/or photo/hydro/thermal degradation (Lakshmipraba, 2024; Liro et al., 2023; Singh & Sharma, 2016). Over time, as plastic size decreases with fragmentation, its abundance exponentially increases and so does its potential to negatively affect ecosystem health (Prata et al., 2024; Weinstein et al., 2022). In addition, MP transport processes (i.e. wind uptake, earthworm movement) vary depending on their shape and size (Rillig et al., 2017; Su et al., 2022; Tatsii et al., 2024). Thus, although the waste caused by macro plastic (>5 mm) debris is more conspicuous, MPs are often more likely to be spread around the world, making them a pollutant in need of an effective tracking methodology (Lv et al., 2021). For decades, plastic research focused on the oceans, in part driven by the discovery of floating oceanic garbage patches, but a recent study done by Gallitelli and Liro (2024) reported that river garbage patches hold more plastics than oceans, albeit scattered over smaller areas. Rivers are a major contributor to oceanic pollution, with global emission estimates between 1.15 and 2.41 MT of plastic waste per year (Lebreton et al., 2017). Nonetheless, plastics traveling through rivers can get trapped in the riverbed, vegetation, riparian banks, and dams along their way downstream (Gallitelli et al., 2020; van Emmerik et al., 2022). Due to these entrapment features, plastics in river systems have only about a 1.5% probability of entering the ocean, with lower probabilities

further upstream compared to rivers closer to the coast (Meijer et al., 2021). Many factors, such as river discharge and morphological characteristics, influence how plastics settle and are mobilized (Prata et al., 2024; Roebroek et al., 2021). Due to their size, it is challenging to monitor MPs in rivers at large spatial scales, and because their potential to damage ecosystem health is high (Lv et al., 2021; Sarkar et al., 2023), research into how they are transported should be further studied.

Past studies have used a variety of *in situ* methods to estimate MP concentrations. The principal ways to collect river surface samples include grab samples, trawl methods, *in situ* sieve collection, and pumps (Delgado-Gallardo et al., 2021). Studies often aim to quantify MP abundance in different parts of a river (surface water, riverbed, riverbank, etc.) (Akdogan & Guven, 2019), and though harmonization is needed, we must also consider that the methodologies used will depend on the research question posed (Mitrano et al., 2023). Each of these methods has its pros and cons, but all are often costly and time- and labor-intensive (Prata et al., 2024). These current methods allow us to understand MP concentration at a specific time and place, but the next step is to better understand how MPs flow through rivers in order to identify sinks, sources, and pathways (Hale et al., 2020; Liro et al., 2023). To do this, spatial and temporal continuity of sampling is needed (Roebroek et al., 2022), which is not feasible using traditional field methods. To address this shortcoming of traditional sampling techniques, our research considers utilizing satellite imagery. For decades, satellite imagery has been used to estimate various water quality (WQ) parameters in rivers. Multispectral satellite remote sensing can retrieve surface reflectance across multiple wavelengths, which can be used to identify spectral variations in water bodies across space and time. So far, there are no studies that have found MP concentrations in water to significantly change its spectral signature. However, if we are able to relate MP concentrations to optically active WQ parameters, we may be able to use the relationship as a proxy to estimate MP

concentrations using remote sensing. There are few studies that have explored MP concentration relationships to various WQ parameters in rivers, such as turbidity, suspended particulate matter, specific conductivity (SPC), chlorophyll-a (Chl-a), and a few others (Buwono et al., 2021; Eamrat et al., 2022; Salas et al., 2022). We hypothesize that, once the relationship between MP concentration and a satellite-observable WQ parameter is established, the satellite's WQ index can be used to extrapolate MP concentrations on river surfaces.

Being able to estimate MP concentrations along rivers using satellite imagery would allow for insight on the spatial and temporal distribution of MPs, which would allow us to better understand how they move through river systems. To our knowledge, Piehl et al. (2020) and Sullivan et al. (2023) have used this methodological framework for remote sensing MP concentrations in rivers using WQ as a proxy, but to our knowledge, this is the first study to implement it in the U.S., in inland rivers, and to follow through on each section of the framework proposed. Our study aims to find a relationship between MP concentrations and observable WQ parameters along the New River in Southwest Virginia. We use this relationship to extrapolate continuous MP proxy estimates along a section of the New River to get a better idea of their hotspots, sources, and pathways. The resulting map would provide spatially contiguous information on MP distribution within the river to the surrounding communities using cost and time-effective methods which could aid mitigation strategies and regulation.

2. Study Area

We focused on two sites along the New River, in southwest Virginia: Kentland Farm and the Radford Municipal Park (see red pins in Figure 1). The New River begins in North Carolina and makes its way north into the Kanawha River which feeds into the Ohio River and eventually connects with the Mississippi River before flowing into the Gulf of Mexico; thus, this field site

represents a far upstream catchment. Kentland Farm represents a rural area, while the Radford Municipal Park represents a semi-urban area with a population of 16,971 (*U.S. Census Bureau QuickFacts*, n.d.). The width of the river at the Kentland and Radford sites is 179.1 and 131.6 meters, respectively, and both are between 1 and 1.5 meters deep. Between the sites, there is a water treatment plant, a munitions plant, and two creeks that feed into the New River, draining from other urban areas, including Blacksburg, VA. Both sites are downstream of the hydroelectric Claytor Dam, which controls the discharge from upstream sites. The Radford and Kentland Farm sites are 9.7 and 32.2 kilometers downstream of the dam, respectively. Our area of interest along the New River drains relatively low order streams, such as the third-order Stroubles Creek which passes through the town of Blacksburg (O'Donnell & Hotchkiss, 2019) home of Virginia Tech. These two sites have distinct characteristics (rural vs semi-urban) setting up a natural laboratory for real-world comparisons.

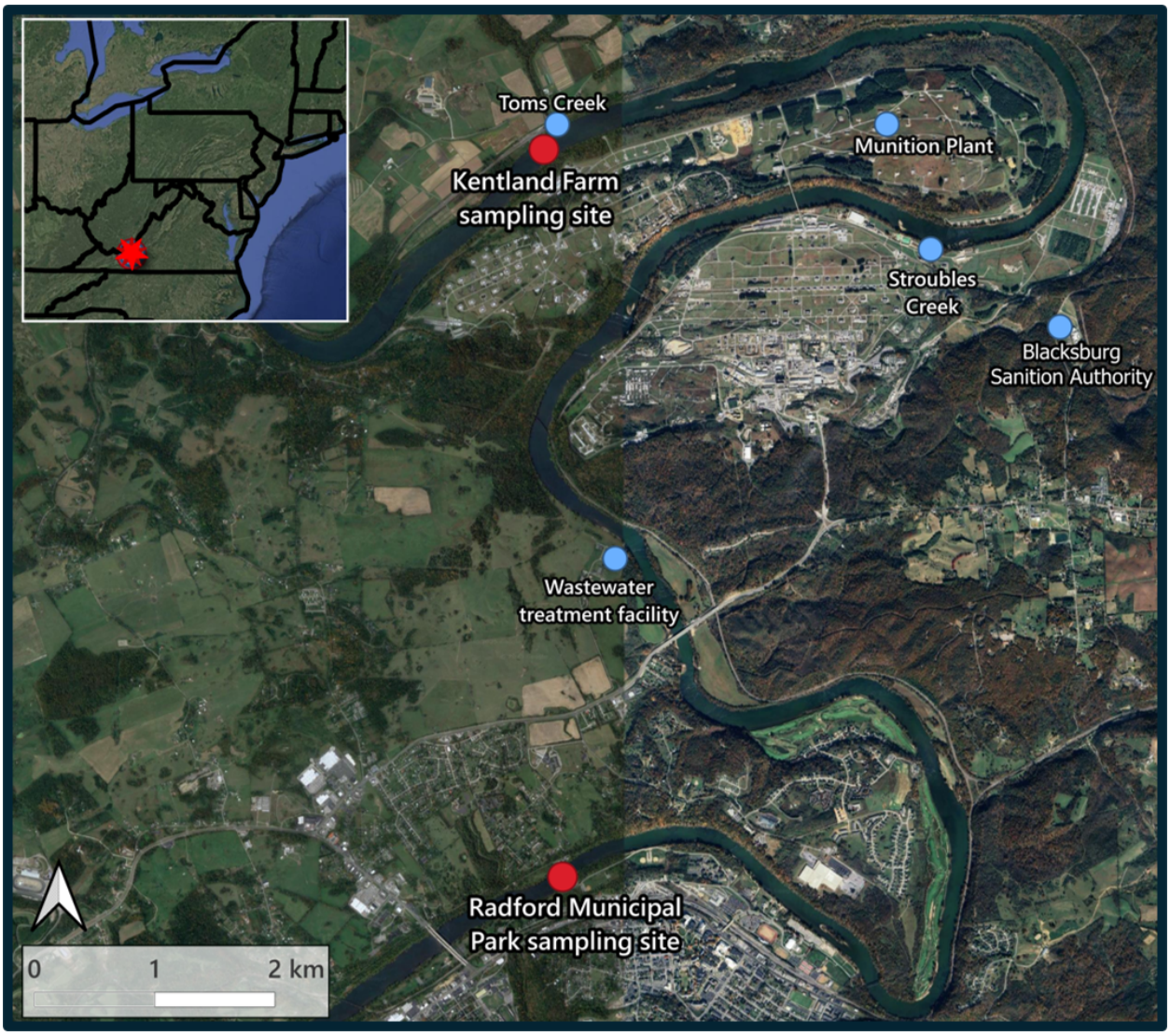

Figure 1. *Two sampling sites in red, and some key features around the sites in blue. The Kentland Farm sampling site is 22.5 kilometers downstream of the Radford Park sampling site.*

3. Methods

3.1 Satellite data collection

Sentinel-2 is a European Space Agency mission with three active satellites that were launched in 2015, 2017, and 2024 (*S2 Mission*, n.d.). During our data collection, we only used Sentinel-2A and 2B. Together, they have a revisit time of 5 days. However, since our field sites were at the

border of two swath paths, we were able to obtain imagery every 2-3 days. Each satellite measures the Earth's reflectance in 12 bands with a spatial resolution of either 10, 60, or 90 meters, depending on the spectral band. Due to its relatively high spatial and temporal resolution, as well as the intersecting swath path over our field area, we decided to use Sentinel-2 imagery to map WQ.

The WQ parameter used to relate to MPs should be based on the context of the field site itself. For our field site, which has relatively low levels and range of Chl-a and SPC, we decided to focus on turbidity. Since turbidity is a measure of particle abundance within the water, it would also be more likely for it to have a relationship with MP abundance. In standard clear water, water reflects low reflectance values in the visible range, with blue reflecting the relatively highest values, then green, then red, and with virtually no reflectance in higher wavelengths (Campbell & Wynne, 2011). Turbidity can be approximated using the normalized difference turbidity index (NDTI) derived by Lacaux et al. (2007), a widely used index in the field. The index capitalizes on the idea that as water becomes more turbid its spectral signature becomes more similar to sediment, which reflects relatively more in the red wavelength range compared to the green band. Due to this, the NDTI takes the normalized difference between the red and green band: $NDTI = \frac{R_{red} - R_{green}}{R_{red} + R_{green}}$,

where R_{red} and R_{green} denotes the red and green wavelength reflectance, respectively. The index ranges from -1 to 1, with clear waters tending towards negative values (green band having higher reflectance than red), and more turbid waters producing higher values (red band reflecting more than green; looking more similar to sediment's signature).

To apply the NDTI to satellite imagery, we first downloaded and processed Sentinel-2 imagery within Google Earth Engine (GEE). We filtered the imagery for our area and dates of interest (2023-09-20 through 2024-09-15). Then, we filtered the collection to only include images with

less than 70% cloud coverage and only include pixels that were classified as “water,” “dark pixels,” “bare soil,” or “vegetation” by Sentinel-2's classification layer, thus omitting “cloud”, and “cloud shadow”. By implementing this method, we ensure an image collection comprised of cloud free pixels for our area of interest. After preprocessing the satellite imagery, we applied the NDTI index throughout the image collection. We then extracted the NDTI values for the points that we sampled in the river and later compared this dataset to the *in situ* turbidity readings to gauge the accuracy of NDTI estimates at our field site, and to establish an equation relating NDTI to *in situ* turbidity (eq.1; see section 3.5).

3.2 Field work

For each sampling day, we collected three co-temporal MP concentration samples and WQ measurements across the rivers’ cross-section on a canoe. At each sample location, we noted the GPS coordinates, took a WQ measurement and a sample of surface water MPs. We used the grab method with a 1L glass-bottle to take MP concentration samples because our research question called for a measurement of MP concentration that is specific to the point where we took WQ measurements. We let the river settle before taking the grab sample and took the sample from the top 10 centimeters of the river. For WQ measurements, we used the Xylem YSI ProDSS Multiparameter Digital Water Quality Meter, which measured depth, temperature, turbidity, dissolved oxygen, SPC, and Chl-a. In total, we collected 110 MP samples and 101 co-temporal WQ measurements. There were fewer WQ measurements than MP samples because the initial 9 field samples were taken without an active YSI. We used the co-temporal WQ and MP datasets to derive a relationship (eq.2) between the two for future MP proxy work (see section 3.5).

We also used the Ocean Optics’ SR4 portable spectrometer to take *in situ* hyperspectral reflectance measurements to compare to the satellite reflectance signature. The equipment was calibrated for

reflectance measurements and taken out in the field to take in situ reflectance measurements from the water's surface. Though the readings were in line with what we would expect for relatively clear waters, taking the equipment onto a canoe in the field was risky and we were not able to capture enough valid measurements to make significant relationships with satellite overpass readings.

3.3 Microplastic isolation and characterization

In the Gray lab at Virginia Tech, we first filtered the MP sample through a 63 μm metal sieve and afterwards digested the sample in 30% hydrogen peroxide to remove organic matter for 48-72 hours (Prata et al., 2019). We then vacuum filtered the sample through a glass flask onto a Sartorius filter with a pore size of 0.45 μm. The filter was transferred into a glass petri dish (60 mmx15 mm VWR) to minimize atmospheric deposition or lab contamination. Over the study, MPs on each filter were enumerated and classified by at least two trained individuals with a Leica S9 stereoscope using the Markley et al. (2024) guidelines, allowing us to distinguish natural from synthetic particles (Gray et al., 2024; Miller et al., 2024). Additionally, MP particles were classified based on color and morphology (fibers, fragments and films). Like previous studies, we only counted MP fibers longer than 300 μm in length (Atwood et al., 2019; Piehl et al., 2020; Sullivan et al., 2023). We also only included MP fragments that were at least 100 μm in width in order to reduce bias for visible particles. Since a particle's size profile influences its movement and how it may impact an ecosystem, we utilized ImageJ, an open-source image processing software, to calculate a subset of particles' aspect ratio (measuring fiber's length:diameter, and fragment and film's length:width) after counting all the filters (Campanale et al., 2020; Rai et al., 2022).

We used a Raman Spectroscopy instrument (Xplora Plus with LabSpec 6 software version 6.5, Horiba Scientific) to confirm polymer composition. Readings were based off a 785 nm or 532 nm laser using gratings of 600 or 1200 grooves/μm, along with 4 accumulations during 4s acquisition times. Spectra were obtained with a hole diameter of 300 μm, a confocal slit width of 100 μm, and using a 10-50x objective with filters ranging from 0.1 to 100% (Gray et al., 2024; Miller et al., 2024). We analyzed 267 of the 4,405 total suspected particles (6%), which is a similar percentage analyzed in previous MP studies (Cowger et al., 2024). Acquired spectra were uploaded to the OpenSpecy software, which determines whether the particle is a plastic by comparing its spectra to a library of lab tested polymer types. We accepted a particle as a plastic polymer if its signature had an R^2 of at least 0.6 that matched with a known polymer (De Frond et al., 2023). Since particles collected in the field have undergone degradation, we assume that their signature will not be the exact same as the lab-tested polymer particle.

3.4 Quality assurance / Quality control

Lab protocols were put in place to minimize contamination, as described in Gray et al. (2024). HEPA filters were kept in each room to reduce atmospheric contamination. DI water was filtered through 0.7 μm GF/C Whatman filters and used to rinse all lab equipment 3x before and after each use. Other than the DI wash bottles (100% LDPE, Fisher Scientific), no plastic was used throughout the procedural steps. Nitrile gloves and 100% cotton lab coats were used during the study (Fisher Scientific). Petri dishes with a Sartorius filter with a pore size of 0.45 μm were set out on either side of the lab work bench to account for atmospheric deposition (4 ± 1 particles/month). We accounted for the influence of background contamination by quantifying procedural blanks (placing filtered DI water through our processing steps), we ran filtered DI water blanks through the same process every 20 samples and recovered an average of 16.9 ± 2.15

particles/blank (mean ± SE; n=8). The MP concentrations that are used for the data analysis and results have been blank adjusted.

3.5 Data Analysis

Other than the preprocessing of satellite imagery with GEE, all data processing and analysis was done in R. From our previous methods, we ended up with three datasets: satellite-derived NDTI, *in situ* turbidity, and MP concentrations at our sample locations. We determined that the distribution of our three datasets did not follow normality using the Shapiro-Wilks test and therefore used the non-parametric Wilcoxon rank-sum-test and the Kruskal-Wallis test along with the Dunn test to check for significant differences between factors such as cross-sectional location and site. We used linear and exponential least square regression techniques to establish relationships between the satellite-derived NDTI and *in situ* turbidity datasets (eq.1) and the *in situ* turbidity and MP concentration datasets (eq.2). We combined Equation 1 and Equation 2 by substituting the *in situ* turbidity variable that is present in both. The combination then produces Equation 3, which relates MP concentration to satellite-derived NDTI, thus allowing us to estimate MP concentration proxy data along rivers from satellite imagery.

4. Results

4.1 Estimating turbidity using NDTI from Sentinel-2

We compared the Sentinel-2 readings to our *in situ* turbidity data to assess whether the satellite-observations corroborate what we measure in the field. After extracting the relevant NDTI values from the satellite imagery, we found 15 cloud-free Sentinel-2 estimates that were co-temporal with our *in situ* data. Fitting a linear regression to the dataset, shown in Figure 2, we found an $R^2 = 0.71$ ($p < 0.001$). Due to the low number of points in the co-temporal overpass dataset ($n = 15$), we also

derived an equation based off valid satellite overpass estimates that were within a day of the *in situ* sampling (n = 43). We fit a linear regression to this dataset, shown in Figure 3, with an $R^2 = 0.41$ ($p < 0.001$). Though this second technique lessens the risk of overfitting a regression, it does introduce a potential error into the relationship since we cannot assume that the conditions within a day of our sampling were similar to the sampling environment during the day of actual sampling. Due to this, we decided to move forward with the first approach for our Equation 1.

$$Turb = 16.58 + 55.73 \cdot NDTI \qquad \textit{(eq.1)}$$

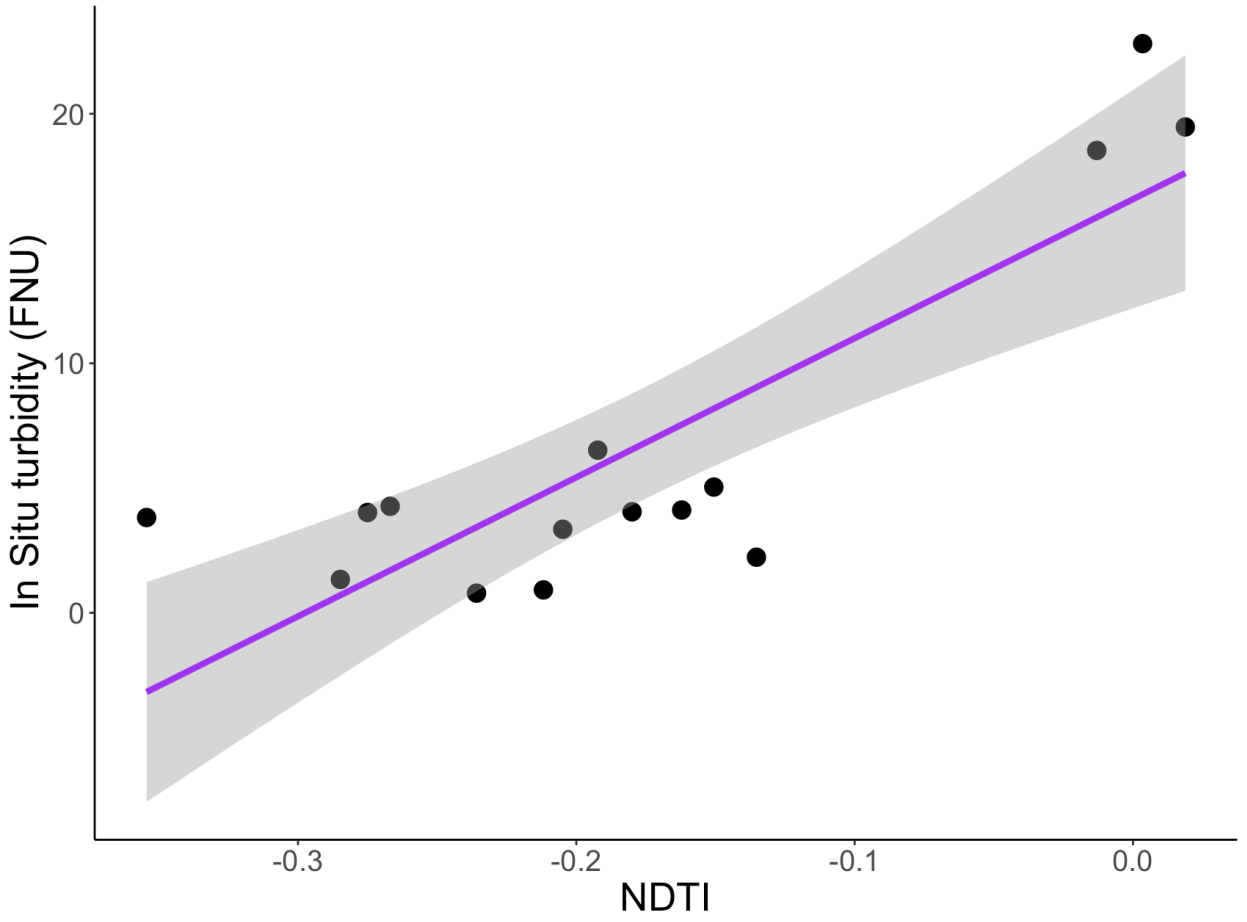

Figure 2: *In situ turbidity (FNU) plotted against same-day satellite-derived NDTI with line of*

*best fit in purple and the 95% confidence interval depicted as the gray shaded boundary (R^2 = 0.71; p <0.01; Turb = 16.58 + 55.73 * NDTI).*

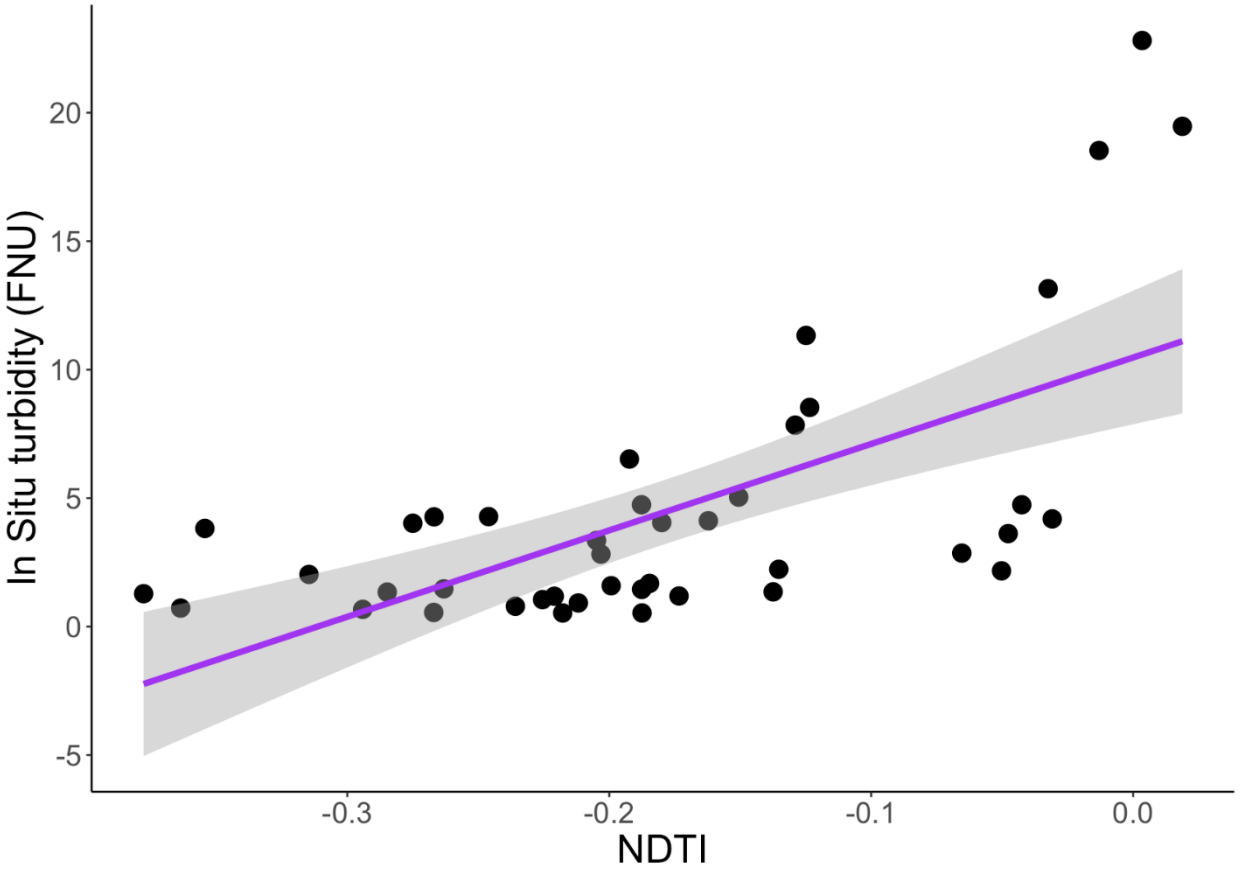

***Figure 3**: Plot shows satellite-derived NDTI taken within a day of in situ turbidity measurements with the line of best fit in purple and the 95% confidence interval depicted as the gray shaded boundary (R^2 = 0.41; p <0.001; In Situ Turbidity (turb) = 10.472 + 33.634 * NDTI).*

4.2 Microplastic characteristics

Of the 110 MP samples taken, eight were taken above the Claytor Dam and seven were tests along the river, both of which were not included in our analysis. This left us with 95 MP samples, and 86 co-temporal water quality measurements, since, as aforementioned, the first nine field samples were taken without an active YSI.

We took a total of 68 samples from the Kentland site throughout the year. We found mean levels of 56.4 ± 6.6 (mean ± SE) MP particles per liter of surface water, with a range between 10 MP/L and 289 MP/L. At the Radford site, we took a total of 27 samples during the winter and spring season. There was an average of 75.3 ± 7.8 (mean ± SE) MP particles per liter of surface water, with a range between 7 MP/L and 163 MP/L. We had fewer Radford samples compared to Kentland because we had conducted an intensive sampling campaign at Kentland Farm starting in the summer and thus discontinued Radford sampling. The purpose of intensive sampling was to be able to take more samples throughout the day to limit other variables, such as weather or discharge, and thus reduce error and capture more variability.

Using the Wilcoxon rank-sum test, we found no significant difference in the amount of MP particles counted or in the turbidity measured between the two sites during the winter and spring (Figure 4; p-value > 0.05). We found no significant difference across each site's cross section (middle, thalweg, and bank) (p-value > 0.05). We also found that the particle characterization distribution was very similar between both sites (Figure 5). Clear/white fibers were the most prevalent in both sites (51% of all Radford particles and 53% of all Kentland particles). Fibers made up roughly 66% of all particles in both sites. On the other hand, films made up 17% of all counted particles in Radford, but only 10% of all particles in Kentland. Only 3% of all particles run on the Raman were found to be other non-plastic material.

The sample with the highest MP/L count was during the summer season, but the winter season samples had a higher average MP/L count, which coincides with higher turbidity and higher discharge during the winter season. There was a peak of fragment abundance during the summer, but it does not seem to align with any significant turbidity nor discharge peaks and thus we

speculate that it could have been due to human activity around that time -- including boating, fishing, and river tubing activity in the area.

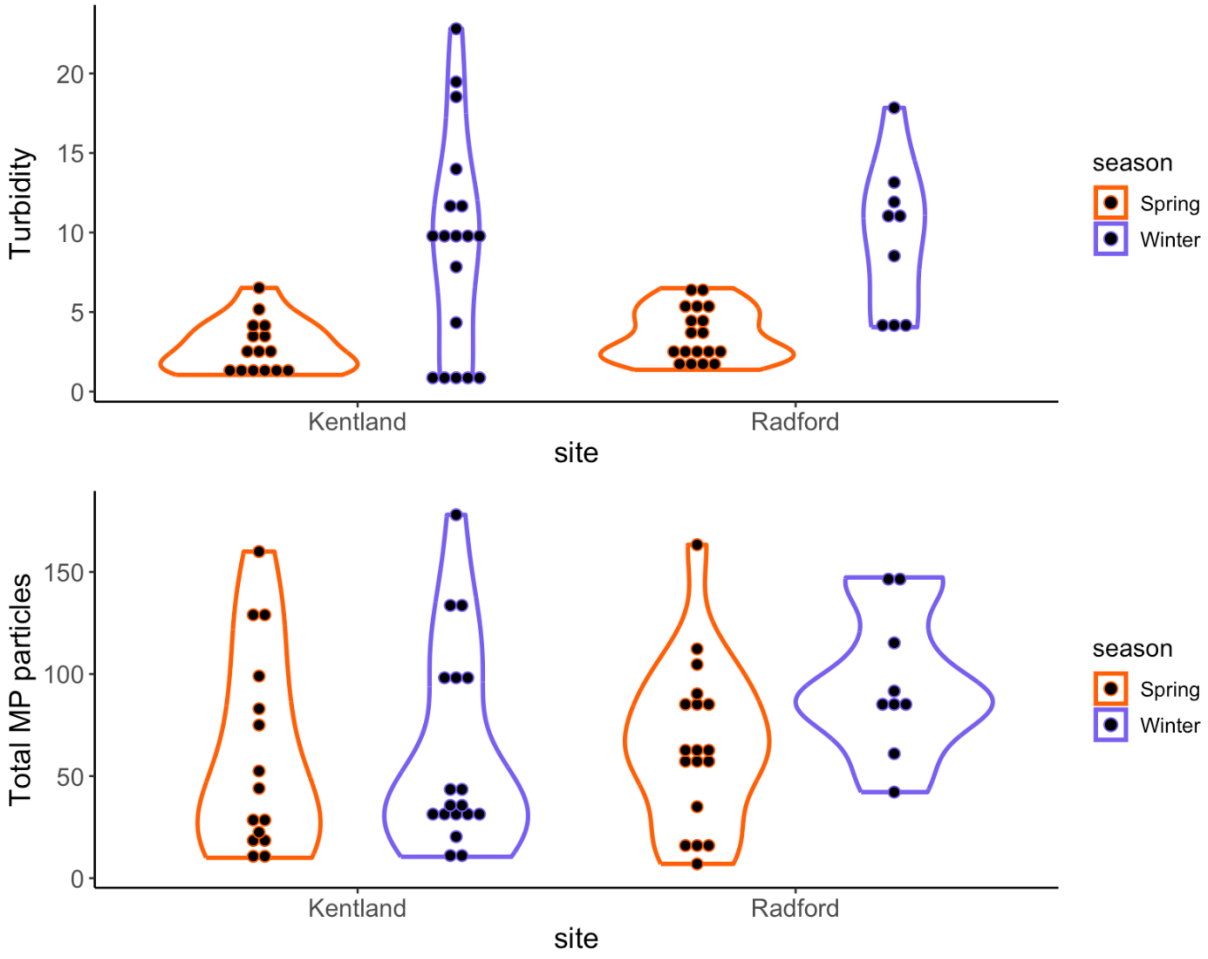

Figure 4*: Violin plots showing the turbidity and total particle counts between the two sites (during the Winter and Spring) showing no significant difference between the two sites during both seasons* ($p > 0.05$).

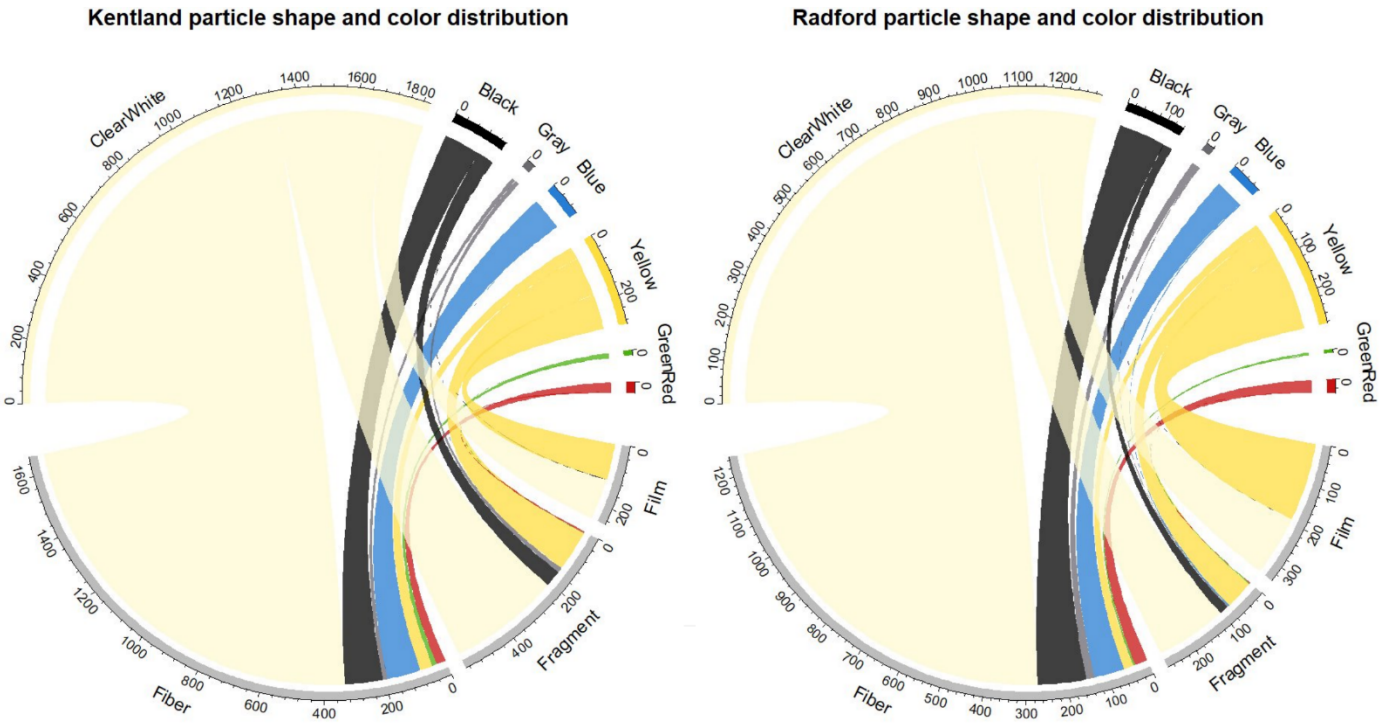

Figure 5*: Chord diagrams for particle shape and color distribution. Particle shape is on the bottom and color is on the top. Lines connecting the categories are by color, and the line width represents the relative amount of the shape-color proportion. The numbers on the perimeter indicate the number of particles in that category.*

Out of the 4,405 particles counted between sites, 2% were taken to be measured using ImageJ (Cowger et al., 2024). On average, fibers had an aspect ratio of 62.61±20.51, fragments had an aspect ratio of 10.1±8.7, and films had an aspect ratio of 1.46±0.02 (mean ± SD). We also ran 10% of all particles on the Raman spectrometer (Figure 6). Of all the particles run on the Raman, 97% were characterized as plastic material. 53% of the Radford particles and 21% of the Kentland particles were identified as polyethylene terephthalate (PET), a thermoplastic polymer under the umbrella of polyester resin, which is often used in textiles, clothes, and packaging (Van Emmerik & Schwarz, 2020). The next most common polymer type was polystyrene within the Radford

particles (8%), and other kinds of plastic within the Kentland particles (7%; other plastics such as polymethylstyrene, acrylonitrile butadiene styrene, polyurethane, etc.).

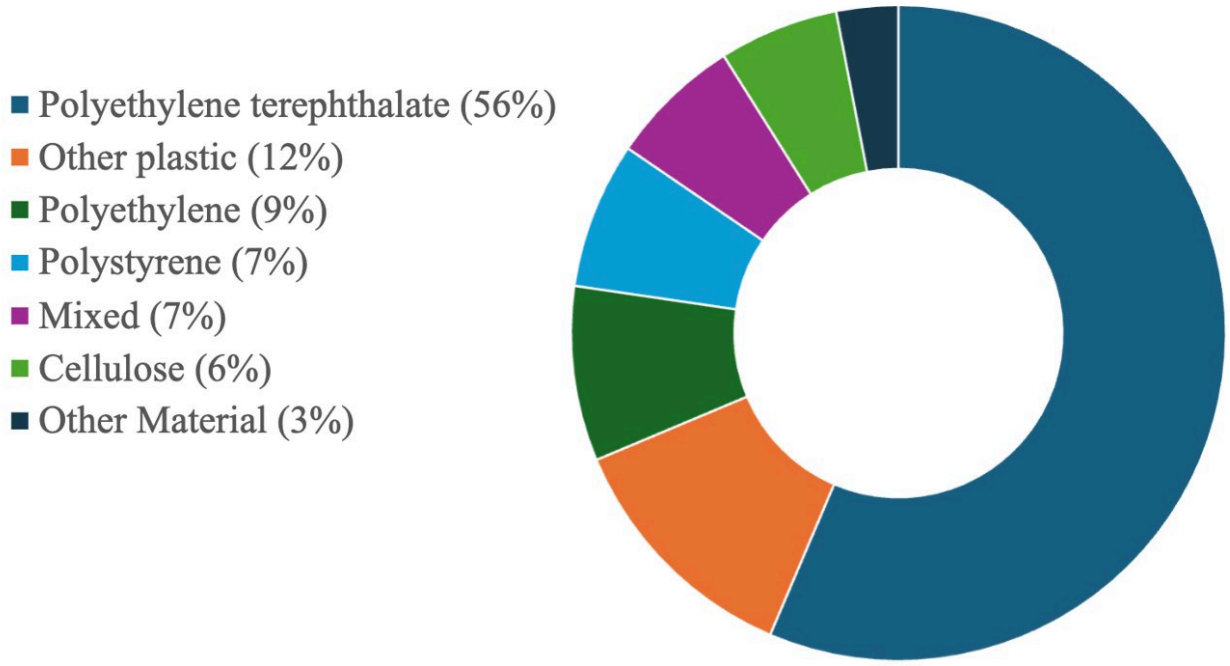

***Figure 6**: Donut chart representing polymer characterization results from Raman Spectrometer.*

4.3 Deriving a relationship between microplastic concentration and turbidity

We explored relationships between MPs and turbidity data using linear and nonlinear regressions for 86 data points (see Methods section 3). Since NDTI was the main parameter that we were able to extract from satellite indices, we only focused on *in situ* turbidity's relationship with MP concentration samples.

The overall relationship between turbidity and total MP concentrations between both sites and for all seasons was best explained using a log-log relationship, seen in Figure 7. The sites are denoted by shape and the seasons are shown in different colors. With the 95 co-temporal points, we found a linear relationship in log-log space with an $R^2 = 0.19$ (eq.2a; p-value < 0.01).

$$\log_{10}(Turbidity) = -0.26 + 0.45 \cdot \log_{10}\left(\frac{MP}{L}\right) \quad \textit{(eq.2a)}$$

Though the R^2 is relatively low, the correlation is positive, which supports our hypothesis that as more MPs are in the water, turbidity will be higher. Highlighting each season by color (Figure 7) also allows us to see clear distinctions between them, so we continued with further seasonal analysis.

In Figure 8, turbidity and the co-temporal total MP particle counts are plotted separately for each season. Here, we confirm that turbidity is noticeably different throughout the seasons, especially between the fall and winter months. We can also see some distinct trends between sites within a given season. For example, during the winter months, Radford had a negative relationship between turbidity and MP counts, while Kentland had a positive relationship. Winter was the season that had the most notably different patterns between sites and yet it is also the season with the highest correlation between turbidity and the MP counted. The entire winter dataset had a linear $R^2 = 0.37$ between MP and turbidity (Figure 8). The relationship between the nine points taken during the winter months in Radford had an $R^2 = 0.62$, while the relationship between the 18 points taken during the winter months in Kentland had an $R^2 = 0.53$.

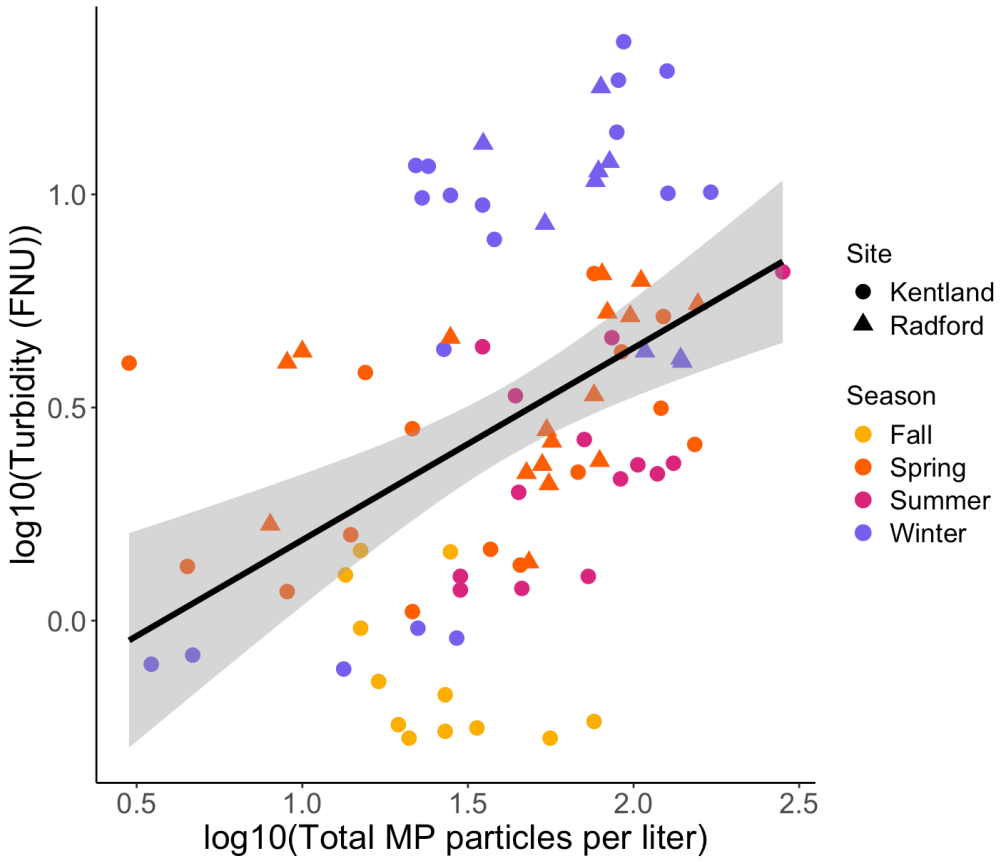

***Figure** 7: Total MP particles per liter against turbidity in log-log space with line of best fit in black and the 95% confidence interval depicted as the gray shaded boundary. Colors correspond to the seasons, and shapes correspond to which site the sample point was taken from ($R2 = 0.19$, $p < 0.001$; $Log_{10}(Turbidity) = -0.26 + 0.45 * log_{10}(MP/L)$.*

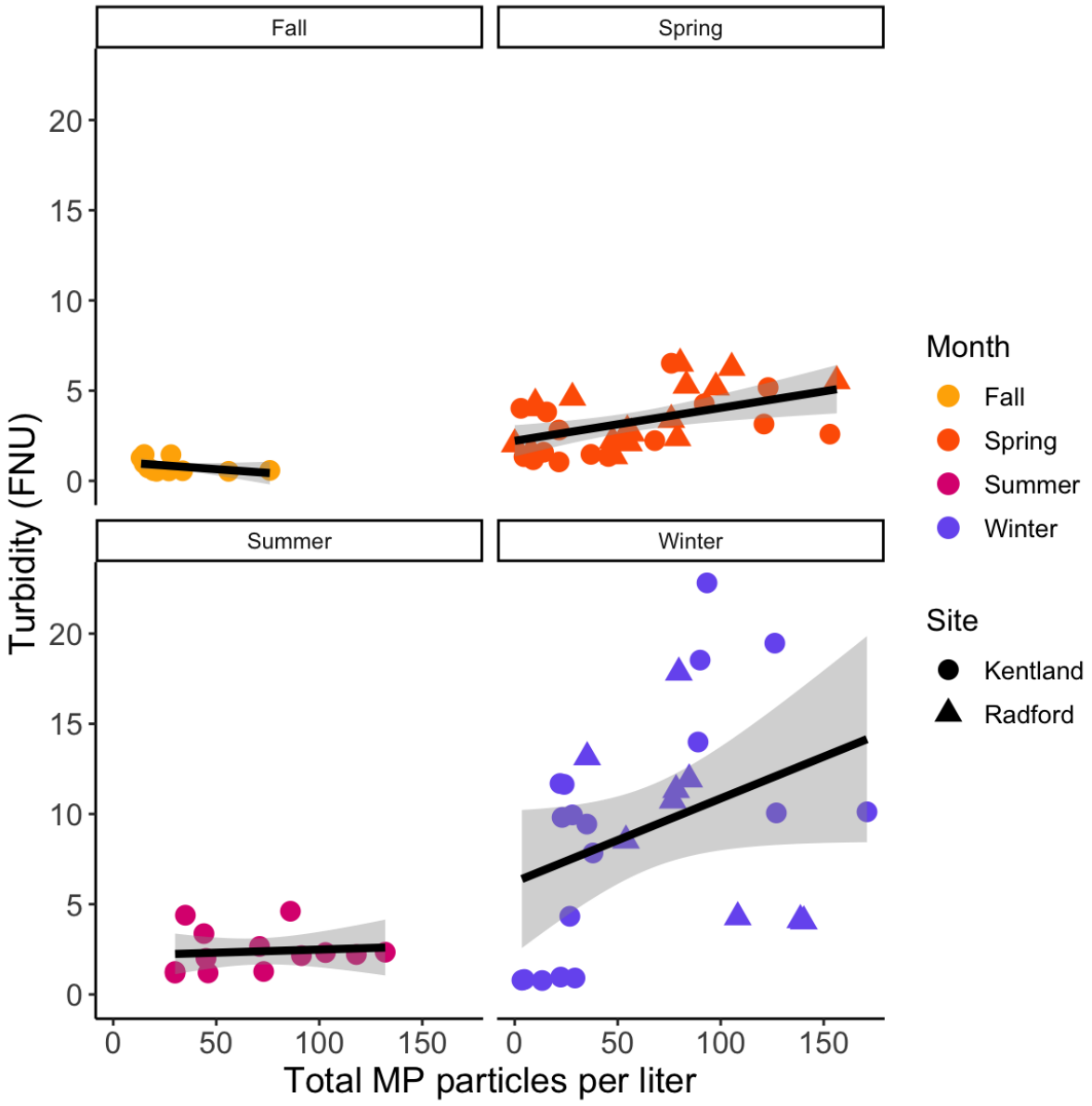

Figure 8: *Total MP particles per liter versus turbidity through different seasons. The line of best fit is shown in black, and the grey shaded area represents the 95% confidence interval. The datapoints also show their site of origin by their shape.*

Microplastic and particle transport along rivers is influenced by discharge, with larger discharge peaks likely remobilizing previously settled material (Karwan & Saiers, 2009; Wagner et al., 2019). Knowing this, we plotted turbidity, MP count per liter, and discharge through time and observed their trends in Figure 9. During January of 2024, there was a relatively large peak in discharge on

the New River, which may have remobilized particles in the river, leading to an increase in turbidity and MP concentrations. Because the winter season covers the largest range in turbidity, and we had more samples in the Kentland Farm area, we decided to further analyze the winter data at Kentland Farm. Focusing on one site also allows us to reduce potential complexities of comparing different sites.

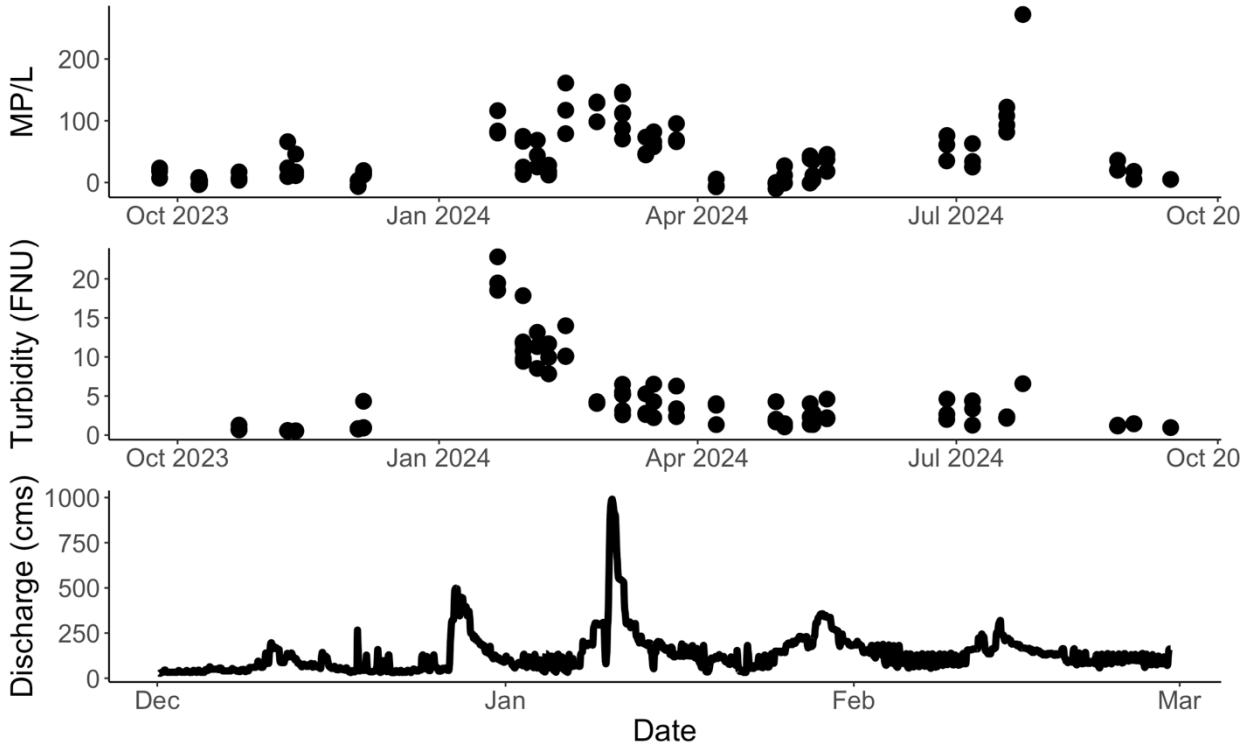

Figure 9*: Plots showing MP/L (top), turbidity (FNU) (middle), and USGS Radford gauge discharge in cubic meters per second (cms) data over our entire field season.*

The winter data at Kentland Farm had the best relationship between turbidity and MP concentration on a log-log scale (Figure 10). We found an R^2 of 0.56 between the 18 co-temporal points using coefficients with a p-value less than 0.05.

$$\log_{10}(Turbidity) = -0.59 + 0.87 \cdot \log_{10}\left(\frac{MP}{L}\right) \qquad \textit{(eq.2b)}$$

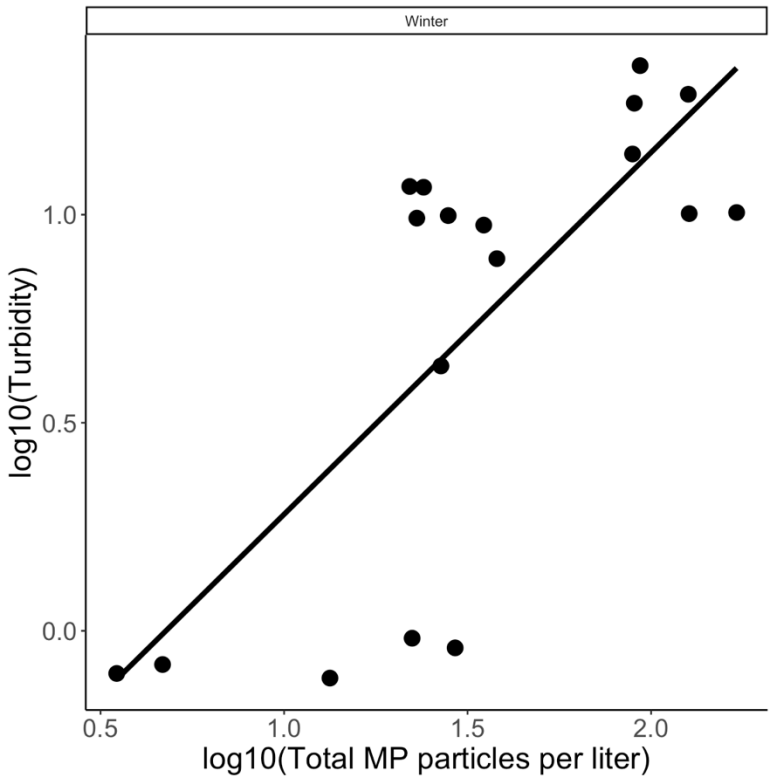

***Figure 10**: MP particles per liter versus turbidity in Kentland during the winter. The line of best fit is shown in black. (R^2 = 0.56; p <0.05; log_{10}(Turbidity) = -0.59 + 0.87 * log_{10}(MP/L).*

4.4 Using turbidity as a proxy for microplastic estimates

To estimate proxy MP concentrations through time and space in our field area, we derived an equation between NDTI versus *in situ* turbidity (eq.1), and *in situ* turbidity versus MP particle concentrations (eq.2a and eq.2b). For the first equation, we utilized the linear equation derived from the same day overpass dataset (n = 15, R^2 = 0.71, p < 0.001), since it explains 71% of the variance. Though our sampling points show relatively low turbidity levels, this linear equation allows for larger turbidity values to be more realistically estimated with NDTI. In contrast, an exponential regression, for example, would not allow for larger turbidity values to be realistically estimated since it will dramatically exaggerate turbidity values associated with higher NDTI values than the range we worked with.

We initially aimed to apply a MP proxy over multiple years and throughout the entire reach of the New River. To do so, we utilized the log-log relationship between turbidity and MP particles using the dataset including all seasons and both sites (n= 95, $R^2 = 0.19$, $p < 0.001$).

Since this produced a low R^2, we explored distinct seasonal analysis and found a significant R^2 during the winter at Kentland Farm (n = 18, $R^2 = 0.56$). Though we won't be able to implement this scenario year-round nor along the entirety of the reach, having a seasonal equation relating MP concentrations to satellite NDTI values does offer more accuracy, and its scale is still larger than what is provided with *in situ* sampling.

Focusing on the larger scale, albeit lower accuracy scenario, we combined Equation 1 and Equation 2a to get Equation 3a. This equation represents MP proxy for the entire field season and both field sites.

$$\frac{MP}{L} = (30.26 + 101.71 \cdot NDTI)^{(2.22)} \qquad \textit{(eq.3a)}$$

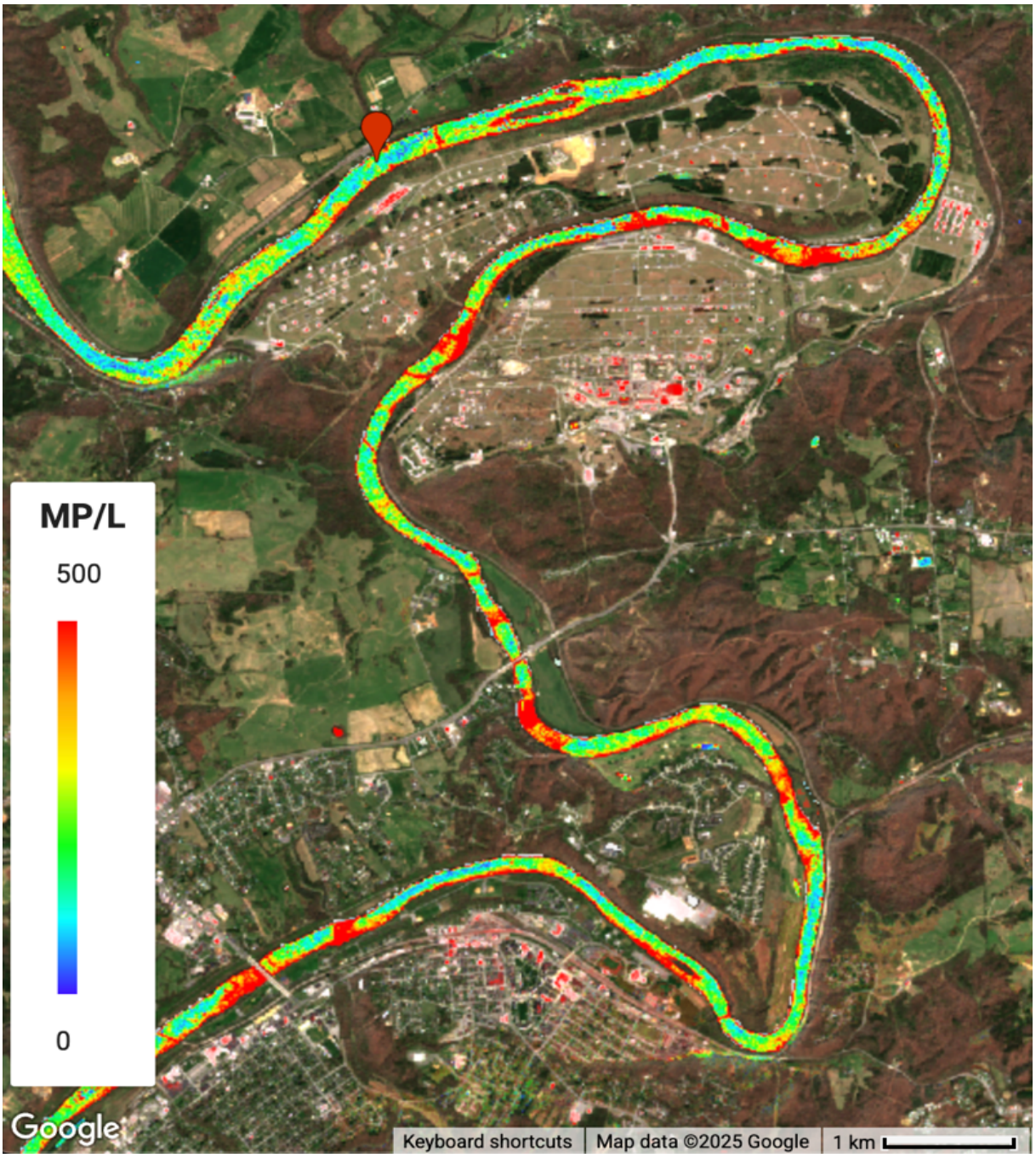

***Figure 11**: Example Sentinel-2 image showing MP concentration proxy values along the New River, VA in April 2024. The color bar is linearly stretched from 0 to 500 MP/L. The Red pin in the northern downstream river denotes where the time series in **Figure 12** was taken.*

Similar to how we mapped NDTI, we applied eq.3a back into GEE and plotted MP proxy values along our field area in the New River (Figure 11) and extrapolated a 5-year time series from September 2019 to September 2024 (Figure 12).

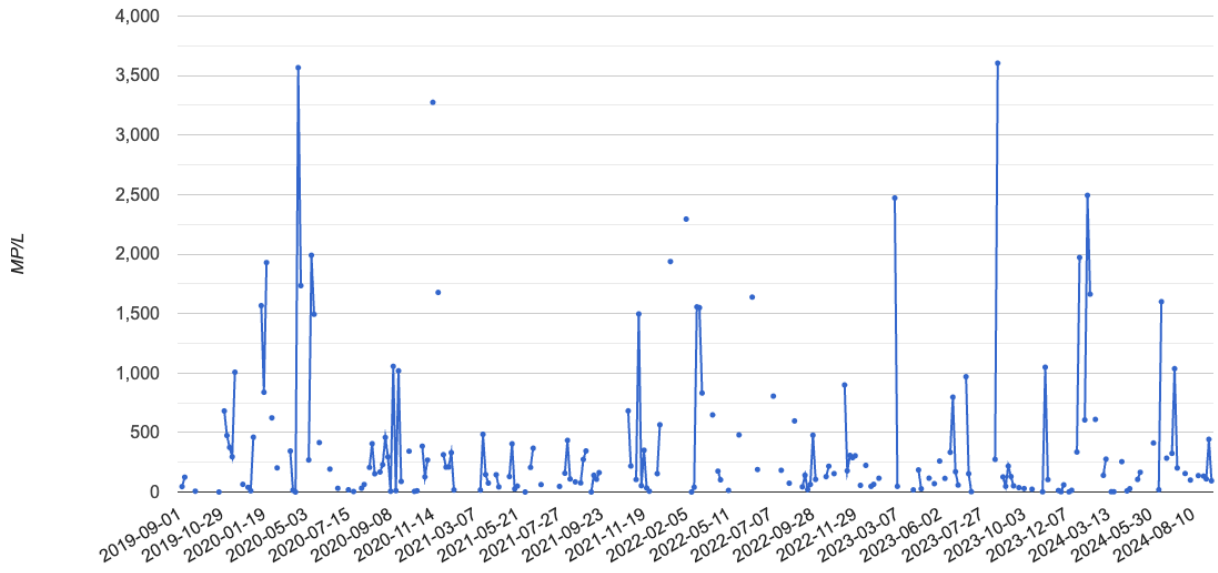

Figure 12**: MP proxy 5-year time series at the red pin shown in **Figure 11.

Focusing on the smaller scale, and at the higher accuracy scenario, we combined Equation 1 and Equation 2b to get Equation 3b. This equation represents MP proxy for the Kentland Farm reach during the winter season.

$$\frac{MP}{L} = (64.45 + 216.66 \cdot NDTI)^{(1.15)} \qquad \textit{(eq.3b)}$$

Like Figures 11 and 12, we applied eq.3b and plotted MP proxy values along the Kentland Farm reach during the winter of 2023-2024 (Figure 13) and got a time series for that period as well (Figure 14).

***Figure 13**: Example Sentinel-2 image showing average MP concentration proxy values along the New River, VA during the winter of 2023-2024. The color bar is linearly stretched from 40 to 150 MP/L. The Red pin denotes where the time series in **Figure 14** was taken.*

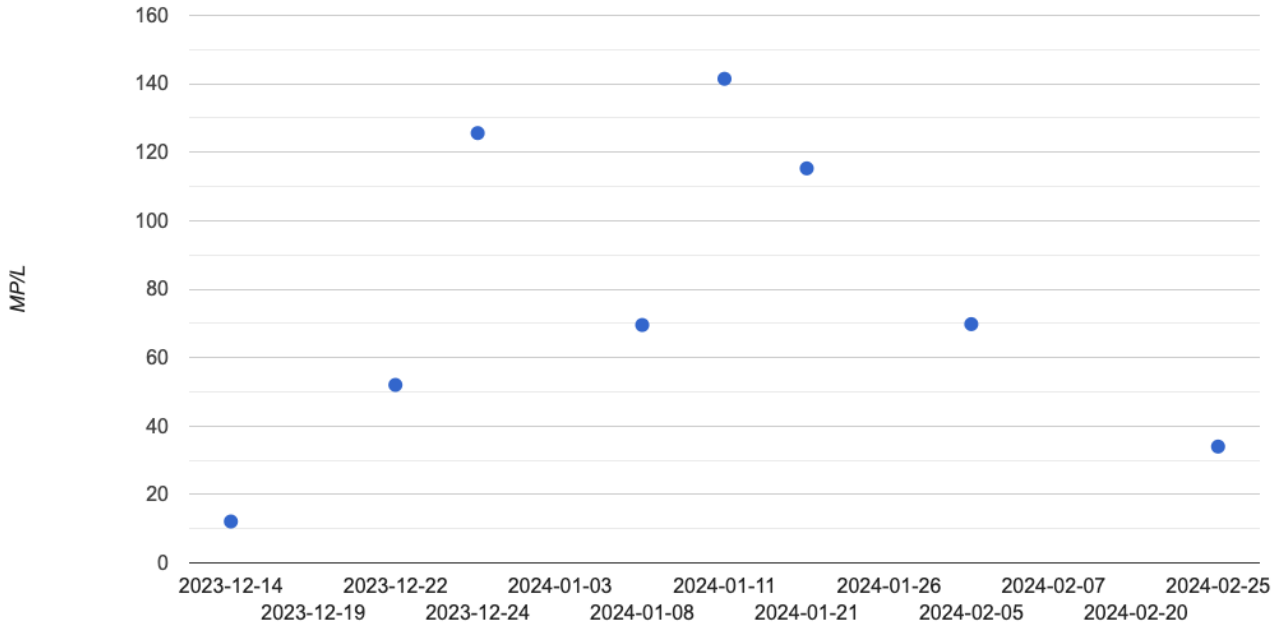

Figure 14: *Time series of MP proxy through the winter of 2023-2024 at the red pin shown in* ***Figure 13.***

4.5 Microplastic proxy accuracy assessment

We conducted an accuracy assessment on the winter at Kentland Farm MP proxy (eq.3b). We chose to only do the accuracy assessment on this scenario because the R^2 for Equation 2b is higher than the R^2 for Equation 2a.

To conduct this accuracy assessment, we extracted the MP proxy values from GEE from the winter analysis (seen through Figure 14). There were 9 points for this section but only 3 of them had co-temporal *in situ* estimates. We plotted these three co-temporal MP proxy and *in situ* MP estimates (Figure 15). Though the R^2 between this is 0.8, the mean square error is very high, indicating poor accuracy (MSE = 374.34 $(MP/L)^2$). However, there are only three points, negating any meaningful interpretation of these statistics.

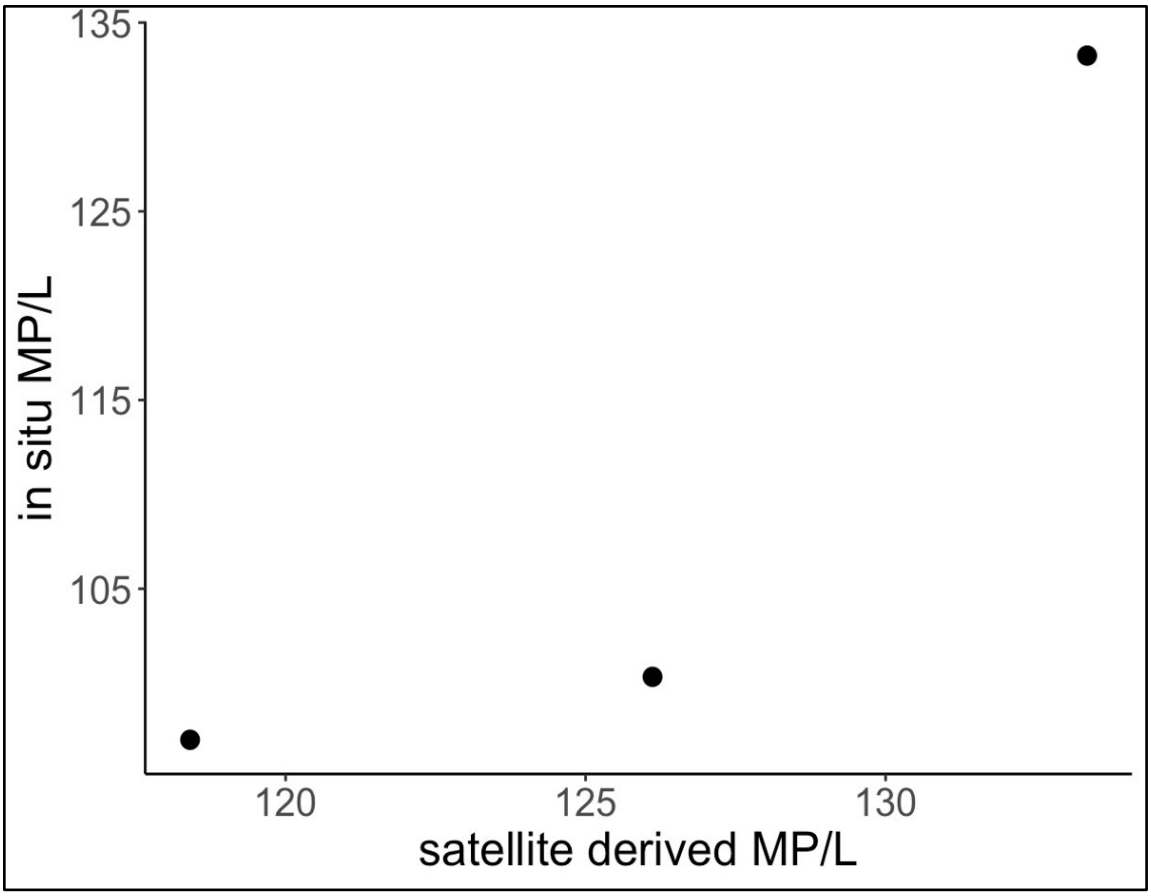

Figure 15: *in situ versus satellite derived proxy MP/L plotted against each other.*

5. Discussion

The section of the New River that contains our field sites has low turbidity, with 77% of our measurements reading under 10 FNU. When plotting against the NDTI values we extracted from satellite imagery, we see the NDTI has a lot of variability along the lower range of turbidity values (Figure 2 and 3). This contrasts with other studies such as Bid and Siddique (2019), which found a significant linear regression ($p < 0.05$) with an R^2 of 0.9 between NDTI and *in situ* turbidity for very turbid rivers in the Panchet Reservoir in India. This may indicate that this kind of analysis is better equipped for rivers which have a wider and a larger range of WQ parameter readings.

Our field area is downstream of the Claytor Dam. Dams significantly affect MP abundance downstream by trapping particles along with sediment (Watkins et al., 2019). Due to this, the MP found in our study sites may not have traveled from far upstream. A recent study by Elnahas et al. (2024) in the same region studied in this paper found that PET was the most prevalent plastic polymer deposited atmospherically. PET was also the most common polymer in our samples (section 4.2). We cannot say with certainty where our plastic particles came from, but having such similar results to an atmospheric deposition study in the same area may allude to high atmospheric deposition rates along the New River.

The MP characterization distribution we found is in line with other studies that also found clear/white fibers to be the most prevalent particle type (Sullivan et al., 2023). This is likely due to the way fibers are transported as they are generally the least dense of the particle shapes (fibers, fragments, and films) (Su et al., 2022). The clear/white coloration is likely due to dye on plastics often being degraded relatively quickly off the particle once in the environment (Zhao et al., 2022). We decided to include size analysis due to recent studies which relate aspect ratio to particle movement, and other studies in the medical field that comment on how aspect ratios can influence MP uptake in the human body, though we did not have the means to further analyze these results (Koelmans et al., 2022; Rosal, 2021).

We found a higher abundance of plastic particles during the summer season, but more fiber particles during the winter season. Sullivan et al. (2023) sampled the Tamar River in northern UK and also found the highest MP amounts during the summer, though their study only included the summer and fall seasons. To our knowledge, there have been no published studies using this method that take MP samples over the entire year. Therefore, we are not able to compare our results with other studies in a robust way.

We found no significant differences between turbidity and total MP count between sites. However, we did find some significant differences in turbidity measurements between seasons. When focusing on the winter season regressions, Kentland exhibited a strong positive relationship, while Radford showed a negative relationship. This discrepancy between sites implies that the turbidity and MP particle relationship may be site specific depending on the site conditions (Piehl et al., 2020). More work and *in situ* measurements would need to be done to implement this kind of work at other sites and at larger scales with higher accuracy.

Following our research question, we used Equation 1 and Equation 2a to derive an equation to extrapolate MP proxy values from satellite imagery over many years and throughout the entire reach of our field sites in the New River, VA. We also used Equation 1 and Equation 2b to extrapolate MP proxy values during the winter throughout the Kentland Farm reach. Though Equation 2b has an R^2 of 0.56, in such a complicated system with many interacting factors, this is a relatively high R^2. In Figure 11, 12, 13, and 14, we see those results. In Figure 11 and 13, we can see the proxy MP mappings along the river surface. In both cases, the edges of the river coincide with higher levels of MP abundance, which is in line with the theory of riverbanks acting as a MP sink due to their high sediment loads and relatively low velocities. We also see this pattern along island banks. There are thin cross-sections of the river indicating very high levels of MPs. This more likely pertains to riffles along the river than a band of concentrated MPs. The New River is very wide and can be 1-1.5 meters deep, but there are many riffles along its path depending on the slope of the terrain. This is a limitation of our study area, since riffles and turbid shallow areas can confound the surface layer river reflectance.

In Figure 12, we see the 5-year time series of the MP proxy estimates. Due to the log-log equation we used (eq.2a), there is a tendency to exaggerate higher values, as we can see by a few readings

above 2,000 MP/L. However, for the most part, the readings lie below 500 MP/L, which is more like what we saw in the field. The winter time series in Figure 14, on the other hand, is consistently more in line with what we found in the field, indicating higher accuracy at smaller scales. Finally, we do not see a long-term trend in the 5-year time series, indicating that the multi-year average in MP abundance has been the same throughout the past 5 years.

Once the MP proxy equation is obtained and plotted both spatially and temporally, its accuracy can be calculated by comparing *in situ* versus proxy estimates (as seen in section 4.5). One can even note that the datapoint on the far-right measures roughly 135 MP/L for both proxy and *in situ* data. Since there are only three points for this accuracy assessment, small deviations get exaggerated when calculating the MSE. Future work should optimize the amount of co-temporal points to best gauge for accuracy.

For future studies, we advise taking an abundance of co-temporal WQ and MP samples over a variety of ranges, such as, seasonal, high and low flow conditions, before and after dam influence, and maybe even at different depths along a larger river reach. This mapping of different relationships at varying river conditions would allow for more accurate and detailed MP concentration mapping along river surfaces. More work should also be done to validate proxy MP results using historical *in situ* MP measurements. Since the MP proxy dataset is plotted at large scales, the *in situ* MP dataset may not be large enough to provide a good accuracy assessment. For this purpose, it is essential to optimize the accuracy of equations used to derive the proxy equation.

6. Conclusions

This study serves as a proof of concept for a novel method to detect MP concentrations along rivers using satellite imagery. We focused on two field sites along the New River, VA, and investigated MP patterns and their relationship to turbidity, as well as the accuracy of satellite readings for

turbidity. We found similar MP characteristics at both our field sites, and no significant difference between turbidity nor MP abundance between the sites. We were able to derive two MP proxy equations from the turbidity-MP observations and later map them through space and create a time series at specific points along the river. This first step towards accurate remote sensing of plastics could help identify MP hotspots which could be point source emissions or sinks and call for more targeted clean-up efforts and mitigation strategies. With more information on MP abundance and its movement throughout the New River, VA, we hope that this method will aid conservancy efforts, and policy and regulation against plastic pollution.

We encourage future studies to implement this method in different regions. Relating MP to various other water properties detectable via satellite imagery at other sites could help better understand what other properties MP act similarly to and what may influence MP concentration in different regions. If this work is implemented on other rivers, it may improve estimate patterns and concentrations of MPs along bodies of water in unmonitored basins. This kind of study pushes forward the effort to implement this cost- and labor-efficient method for tracking MP along rivers worldwide.

References

Akdogan, Z., & Guven, B. (2019). Microplastics in the environment: A critical review of current understanding and identification of future research needs. *Environmental Pollution*, *254*, 113011. https://doi.org/10.1016/j.envpol.2019.113011

Atwood, E. C., Falcieri, F. M., Piehl, S., Bochow, M., Matthies, M., Franke, J., Carniel, S., Sclavo, M., Laforsch, C., & Siegert, F. (2019). Coastal accumulation of microplastic particles emitted from the Po River, Northern Italy: Comparing remote sensing and hydrodynamic modelling with in situ sample collections. *Marine Pollution Bulletin*, *138*, 561–574. https://doi.org/10.1016/j.marpolbul.2018.11.045

Bid, S., & Siddique, G. (2019). Identification of seasonal variation of water turbidity using NDTI method in Panchet Hill Dam, India. *Modeling Earth Systems and Environment*, *5*(4), 1179–1200. https://doi.org/10.1007/s40808-019-00609-8

Buwono, N. R., Risjani, Y., & Soegianto, A. (2021). Distribution of microplastic in relation to water quality parameters in the Brantas River, East Java, Indonesia. *Environmental Technology & Innovation*, *24*, 101915. https://doi.org/10.1016/j.eti.2021.101915

Campanale, C., Massarelli, C., Savino, I., Locaputo, V., & Uricchio, V. F. (2020). A Detailed Review Study on Potential Effects of Microplastics and Additives of Concern on Human Health. *International Journal of Environmental Research and Public Health*, *17*(4), 1212. https://doi.org/10.3390/ijerph17041212

Campbell, J. B., & Wynne, R. H. (2011). *Introduction to Remote Sensing, Fifth Edition*. Guilford Press.

Cowger, W., Markley, L. A. T., Moore, S., Gray, A. B., Upadhyay, K., & Koelmans, A. A. (2024). How many microplastics do you need to (sub)sample? *Ecotoxicology and Environmental Safety*, *275*, 116243. https://doi.org/10.1016/j.ecoenv.2024.116243

De Frond, H., Cowger, W., Renick, V., Brander, S., Primpke, S., Sukumaran, S., Elkhatib, D., Barnett, S., Navas-Moreno, M., Rickabaugh, K., Vollnhals, F., O'Donnell, B., Lusher, A., Lee, E., Lao, W., Amarpuri, G., Sarau, G., & Christiansen, S. (2023). What determines accuracy of chemical identification when using microspectroscopy for the analysis of microplastics? *Chemosphere*, *313*, 137300. https://doi.org/10.1016/j.chemosphere.2022.137300

Delgado-Gallardo, J., Sullivan, G. L., Esteban, P., Wang, Z., Arar, O., Li, Z., Watson, T. M., & Sarp, S. (2021). From Sampling to Analysis: A Critical Review of Techniques Used in the Detection of Micro- and Nanoplastics in Aquatic Environments. *ACS ES&T Water*, *1*(4), 748–764. https://doi.org/10.1021/acsestwater.0c00228

Eamrat, R., Taweesan, A., & Pussayanavin, T. (2022). Assessment of Microplastics Distribution and Related Water Quality in an Urban Canal Thailand. *Pollution*, *8*(4). https://doi.org/10.22059/poll.2022.340679.1407

Elnahas, A., Gray, A., Lee, J., AlAmiri, N., Pokhrel, N., Allen, S., & Foroutan, H. (2025). Atmospheric Deposition of Microplastics in South Central Appalachia in the United States. *ACS ES&T Air*, *2*(1), 64–72. https://doi.org/10.1021/acsestair.4c00189

Gallitelli, L., Cesarini, G., Cera, A., Sighicelli, M., Lecce, F., Menegoni, P., & Scalici, M. (2020). Transport and Deposition of Microplastics and Mesoplastics along the River Course: A Case Study of a Small River in Central Italy. *Hydrology*, *7*(4), 90. https://doi.org/10.3390/hydrology7040090

Gallitelli, L., & Liro, M. (2024). Do river garbage patches exist? *Frontiers in Environmental Science*, *12*, 1480391. https://doi.org/10.3389/fenvs.2024.1480391

Geyer, R., Jambeck, J. R., & Law, K. L. (2017). Production, use, and fate of all plastics ever made. *Science Advances*, *3*(7), e1700782. https://doi.org/10.1126/sciadv.1700782

Gray, A., Mayer, K., Gore, B., Gaesser, M., & Ferguson, N. (2024). Microplastic burden in native (Cambarus appalachiensis) and non-native (Faxonius cristavarius) crayfish along semi-rural and urban streams in southwest Virginia, USA. *Environmental Research*, *258*, 119494. https://doi.org/10.1016/j.envres.2024.119494

Hale, R. C., Seeley, M. E., La Guardia, M. J., Mai, L., & Zeng, E. Y. (2020). A Global Perspective on Microplastics. *Journal of Geophysical Research: Oceans*, *125*(1), e2018JC014719. https://doi.org/10.1029/2018JC014719

Karwan, D. L., & Saiers, J. E. (2009). Influences of seasonal flow regime on the fate and transport of fine particles and a dissolved solute in a New England stream. *Water Resources Research*, *45*(11), 2009WR008077. https://doi.org/10.1029/2009WR008077

Koelmans, A. A., Redondo-Hasselerharm, P. E., Nor, N. H. M., de Ruijter, V. N., Mintenig, S. M., & Kooi, M. (2022). Risk assessment of microplastic particles. *Nature Reviews Materials*, *7*(2), 138–152. https://doi.org/10.1038/s41578-021-00411-y

Lacaux, J. P., Tourre, Y. M., Vignolles, C., Ndione, J. A., & Lafaye, M. (2007). Classification of ponds from high-spatial resolution remote sensing: Application to Rift Valley Fever epidemics in Senegal. *Remote Sensing of Environment*, *106*(1), 66–74. https://doi.org/10.1016/j.rse.2006.07.012

Lakshmipraba, J. (2024). Photo/Hydro/Thermal Degradation of Macro-plastics into Micro- and Nano-forms. In V. Sivasankar & T. G. Sunitha (Eds.), *Microplastics and Pollutants: Interactions, Degradations and Mechanisms* (pp. 51–74). Springer Nature Switzerland. https://doi.org/10.1007/978-3-031-54565-8_3

Lebreton, L. C. M., Van Der Zwet, J., Damsteeg, J.-W., Slat, B., Andrady, A., & Reisser, J. (2017). River plastic emissions to the world's oceans. *Nature Communications*, *8*(1), 15611. https://doi.org/10.1038/ncomms15611

Lindeque, P. K., Cole, M., Coppock, R. L., Lewis, C. N., Miller, R. Z., Watts, A. J. R., Wilson-McNeal, A., Wright, S. L., & Galloway, T. S. (2020). Are we underestimating microplastic abundance in the marine environment? A comparison of microplastic capture with nets of different mesh-size. *Environmental Pollution*, *265*, 114721. https://doi.org/10.1016/j.envpol.2020.114721

Liro, M., Zielonka, A., & Van Emmerik, T. H. M. (2023). Macroplastic fragmentation in rivers. *Environment International*, *180*, 108186. https://doi.org/10.1016/j.envint.2023.108186

Meijer, L. J. J., Van Emmerik, T., Van Der Ent, R., Schmidt, C., & Lebreton, L. (2021). More than 1000 rivers account for 80% of global riverine plastic emissions into the ocean. *Science Advances*, *7*(18), eaaz5803. https://doi.org/10.1126/sciadv.aaz5803

Miller, J., Barrett, N., Love, J., Gray, A., Youker, R., Hall, C., Meiri, N., Gaesser, M., Randall, G., Jarrett, R., & Spafford, J. (2024). Temporal and Spatial Variations in Microplastic Concentrations in Small Headwater Basins in the Southern Blue Ridge Mountains, North Carolina, USA. *Environments*, *11*(11), 240. https://doi.org/10.3390/environments11110240

Mitrano, D. M., Diamond, M. L., Kim, J.-H., Tam, K. C., Yang, M., & Wang, Z. (2023). Balancing New Approaches and Harmonized Techniques in Nano- and Microplastics Research. *Environmental Science & Technology*, *57*(24), 8841–8844. https://doi.org/10.1021/acs.est.3c04120

O'Donnell, B., & Hotchkiss, E. R. (2019). Coupling Concentration- and Process-Discharge Relationships Integrates Water Chemistry and Metabolism in Streams. *Water Resources Research*, *55*(12), 10179–10190. https://doi.org/10.1029/2019WR025025

OECD. (2024). *Policy Scenarios for Eliminating Plastic Pollution by 2040*. OECD. https://doi.org/10.1787/76400890-en

Piehl, S., Atwood, E. C., Bochow, M., Imhof, H. K., Franke, J., Siegert, F., & Laforsch, C. (2020). Can Water Constituents Be Used as Proxy to Map Microplastic Dispersal Within Transitional and Coastal Waters? *Frontiers in Environmental Science*, *8*, 92. https://doi.org/10.3389/fenvs.2020.00092

Prata, J. C., da Costa, J. P., Girão, A. V., Lopes, I., Duarte, A. C., & Rocha-Santos, T. (2019). Identifying a quick and efficient method of removing organic matter without damaging microplastic samples. *Science of The Total Environment*, *686*, 131–139. https://doi.org/10.1016/j.scitotenv.2019.05.456

Prata, J. C., Padrão, J., Khan, M. T., & Walker, T. R. (2024). Do's and don'ts of microplastic research: A comprehensive guide. *Water Emerging Contaminants & Nanoplastics*, *3*(21). https://doi.org/10.20517/wecn.2023.61

Rai, P. K., Sonne, C., Brown, R. J. C., Younis, S. A., & Kim, K.-H. (2022). Adsorption of environmental contaminants on micro- and nano-scale plastic polymers and the influence of weathering processes on their adsorptive attributes. *Journal of Hazardous Materials*, *427*, 127903. https://doi.org/10.1016/j.jhazmat.2021.127903

Rillig, M. C., Ziersch, L., & Hempel, S. (2017). Microplastic transport in soil by earthworms. *Scientific Reports*, *7*(1), 1362. https://doi.org/10.1038/s41598-017-01594-7

Roebroek, C. T. J., Harrigan, S., Van Emmerik, T. H. M., Baugh, C., Eilander, D., Prudhomme, C., & Pappenberger, F. (2021). Plastic in global rivers: Are floods making it worse? *Environmental Research Letters*, *16*(2), 025003. https://doi.org/10.1088/1748-9326/abd5df

Roebroek, C. T. J., Laufkötter, C., González-Fernández, D., & Van Emmerik, T. (2022). The quest for the missing plastics: Large uncertainties in river plastic export into the sea. *Environmental Pollution*, *312*, 119948. https://doi.org/10.1016/j.envpol.2022.119948

Rosal, R. (2021). Morphological description of microplastic particles for environmental fate studies. *Marine Pollution Bulletin*, *171*, 112716. https://doi.org/10.1016/j.marpolbul.2021.112716

S2 Mission. (n.d.). Retrieved January 28, 2025, from https://sentiwiki.copernicus.eu/web/s2-mission

Salas, E. A. L., Kumaran, S. S., Partee, E. B., Willis, L. P., & Mitchell, K. (2022). Potential of mapping dissolved oxygen in the Little Miami River using Sentinel-2 images and machine learning algorithms. *Remote Sensing Applications: Society and Environment*, *26*, 100759. https://doi.org/10.1016/j.rsase.2022.100759

Sarkar, S., Diab, H., & Thompson, J. (2023). Microplastic Pollution: Chemical Characterization and Impact on Wildlife. *International Journal of Environmental Research and Public Health*, *20*(3), 1745. https://doi.org/10.3390/ijerph20031745

Singh, P., & Sharma, V. P. (2016). Integrated Plastic Waste Management: Environmental and Improved Health Approaches. *Procedia Environmental Sciences*, *35*, 692–700. https://doi.org/10.1016/j.proenv.2016.07.068

Su, L., Xiong, X., Zhang, Y., Wu, C., Xu, X., Sun, C., & Shi, H. (2022). Global transportation of plastics and microplastics: A critical review of pathways and influences. *Science of The Total Environment*, *831*, 154884. https://doi.org/10.1016/j.scitotenv.2022.154884

Sullivan, E., Cole, M., Atwood, E. C., Lindeque, P. K., Chin, P. T., & Martinez-Vicente, V. (2023). In situ correlation between microplastic and suspended particulate matter concentrations in river-estuary systems support proxies for satellite-derived estimates of microplastic flux. *Marine Pollution Bulletin*, *196*, 115529. https://doi.org/10.1016/j.marpolbul.2023.115529

Tatsii, D., Bucci, S., Bhowmick, T., Guettler, J., Bakels, L., Bagheri, G., & Stohl, A. (2024). Shape Matters: Long-Range Transport of Microplastic Fibers in the Atmosphere. *Environmental Science & Technology*, *58*(1), 671–682. https://doi.org/10.1021/acs.est.3c08209

U.S. Census Bureau QuickFacts: Radford city, Virginia. (n.d.). Retrieved January 28, 2025, from https://www.census.gov/quickfacts/fact/table/radfordcityvirginia/PST045223#PST045223

van Emmerik, T., Mellink, Y., Hauk, R., Waldschläger, K., & Schreyers, L. (2022). *Rivers as Plastic Reservoirs*. *3*. https://doi.org/10.3389/frwa.2021.786936

Van Emmerik, T., & Schwarz, A. (2020). Plastic debris in rivers. *WIREs Water*, *7*(1), e1398. https://doi.org/10.1002/wat2.1398

Wagner, S., Klöckner, P., Stier, B., Römer, M., Seiwert, B., Reemtsma, T., & Schmidt, C. (2019). Relationship between Discharge and River Plastic Concentrations in a Rural and an Urban Catchment. *Environmental Science & Technology*, *53*(17), 10082–10091. https://doi.org/10.1021/acs.est.9b03048

Watkins, L., McGrattan, S., Sullivan, P. J., & Walter, M. T. (2019). The effect of dams on river transport of microplastic pollution. *Science of The Total Environment*, *664*, 834–840. https://doi.org/10.1016/j.scitotenv.2019.02.028

Weinstein, J. E., Ertel, B. M., & Gray, A. D. (2022). Accumulation and depuration of microplastic fibers, fragments, and tire particles in the eastern oyster, Crassostrea virginica: A toxicokinetic approach. *Environmental Pollution*, *308*, 119681. https://doi.org/10.1016/j.envpol.2022.119681

Zhao, X., Wang, J., Yee Leung, K. M., & Wu, F. (2022). Color: An Important but Overlooked Factor for Plastic Photoaging and Microplastic Formation. *Environmental Science & Technology*, *56*(13), 9161–9163. https://doi.org/10.1021/acs.est.2c02402